Journal Name

RSC**Publishing**

COMMUNICATION

A high efficiency H$_2$S gas sensor material: Paper like Fe$_2$O$_3$/Graphene nanosheets and structural alignment dependency of device efficiency

Zaixing Jiang,[a,b,†] Jun Li,[a,†] Hüsnü Aslan,[b,†] Qiang Li,[b] Yue Li,[a] Menglin Chen,[b] Yudong Huang,[a,*] Jens Peter Froning,[c] Michal Otyepka,[c] Radek Zbořil,[c] Flemming Besenbacher,[b] Mingdong Dong[b,*]

The Fe$_2$O$_3$/Graphene were synthesized successfully by super critical CO$_2$-assisted thermal method and further produced into paper-like nanosheets by directed-flow, vertical assembly of individual Fe$_2$O$_3$/Graphene nanosheets under controlled magnetic field. Characterizations of the samples were carried out by both electron microscopy and X-ray photoelectron spectroscopy. The sensor materials outperform many other paper-like materials in response to H$_2$S gas detection. In addition, vertically and horizontally aligned nanosheets were used as sensing materials to detect H$_2$S gas along with chemiluminescence measurements. Importantly, the nanoscale Fe$_2$O$_3$/Graphene sheets with the vertical arrangement are more beneficial than the nanosheets with the horizontal arrangement in terms of sensitivity.

Inorganic paper-like materials based on nanoscale components are a growing field of research due to their vast variety of applications in technology such as protective layers, chemical filters, components of electrical batteries or supercapacitors, adhesive layers, electronic or optoelectronic components, and molecular storage.[1-3] However, preparation of the paper-like materials, on which their components are perpendicular to its surface, has remained elusive so far. Considering most of the applications of so called paper-like materials are depending on their surface area and alignment of the active interface, using vertically nanostructures to produce these papers would significantly increase the total area of reaction as they are parallel to the flow of signal source (chemicals, biomaterials, radiation etc.) hence enhance the yield of the desired application. [4-6]

Herein, we report paper like preparation of vertically arranged Fe$_2$O$_3$/Graphene nanosheets (VAFe/GN) and horizontally arranged Fe$_2$O$_3$/Graphene nanosheets (HAFe/GN) to be used as H$_2$S sensors. Our motivation to use graphene was not only due to its well-known excellent mechanical and electrical properties but also due to its ultra-low thickness that allows us to have very wide surface areas.[7-12] As one of the most important industry materials, ferric oxide has wide promising applications in catalysts, color finish material, paint, rubber industry and drug carriers.[13-15] But regardless of these applications our reason to prefer ferric oxide was, as recently discovered, its ability to efficiently detect hydrogen sulfide on the basis of chemiluminescent (CL) signal from the intermediate H$_2$S oxidation[16] and its magnetic property which helped us align the Fe$_2$O$_3$/Graphene nanosheets vertically or horizontally under controlled magnetic field.

Initially we started to prepare VAFe/GN paper; its fabrication was carried out in two steps (see Supporting Information, experimental details): i) Graphene oxide (GO) was synthesized by a modified

Hummers method. In a typical experiment to prepare the Fe_2O_3/Graphene nanocomposite, about 2.0 mmol of $Fe(NO_3)_3 \cdot 9H_2O$ was added to 25.0 mL of GO ethanol solution in which $Fe(NO_3)_3$ acted as a precursor to synthesize Fe_2O_3, and the GO acted as a

of magnetic field is parallel to the solution surface), the HAFe/GN could be fabricated.
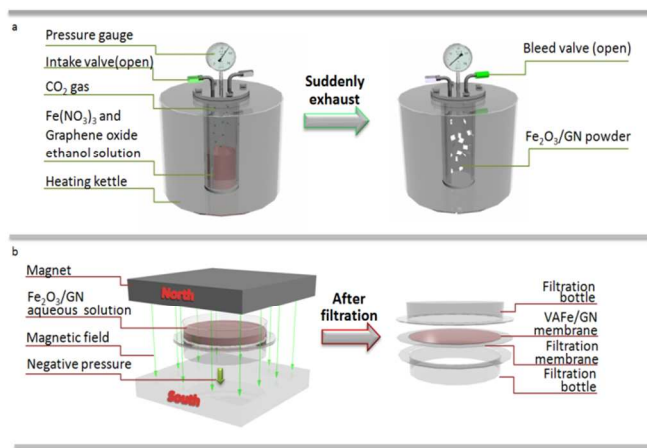

Figure 1. Schematic diagram of Fe_2O_3/Graphene nanocomposite film preparation: (a) fabrication of the Fe_2O_3/Graphene nanosheets; (b) vertical magnetic field assembly method with directed-flow.

substrate to form Fe_2O_3/Graphene nanocomposite. The reactive mixture was ultrasonicated (500 W) for 30 min to obtain homogeneity. Then, the mixture was moved to a 80.0 mL stainless steel vessel. And the vessel was pressurized with super critical (SC) CO_2 up to 5.0 MPa at 0 ℃. After that, the vessel was sealed and moved to an oven at 120 ℃ and maintained at this temperature for 2 h. Subsequently, the vessel was put into a salt-bath furnace at 350 ℃ and kept there for an hour (Figure 1a). After it was cooled to ambient temperature, the vessel was suddenly depressurized, and the black powder of Fe_2O_3/Graphene nanosheets was produced. ii) 200.0 mg of this black powder was re-dispersed in water by ultrasonicating. These Fe_2O_3/Graphene nanosheets could be aligned under directed-flow, controlled magnetic field due to the paramagnetism of Fe_2O_3. Vacuum filtration of colloidal dispersions of Fe_2O_3/Graphene nanosheets through an Anodisc membrane filter under vertical magnetic field yielded, after drying, VAFe/GN paper with thicknesses ranging from 4 to 6 μm (Figure 1b). Through the same procedure, only changing the direction of the magnet (the direction
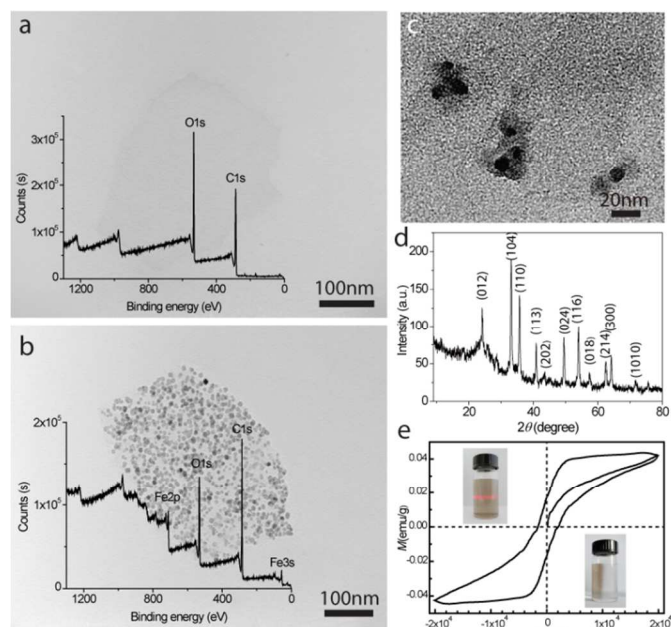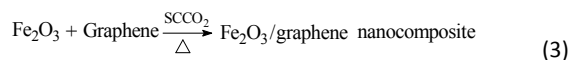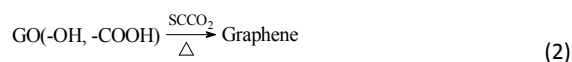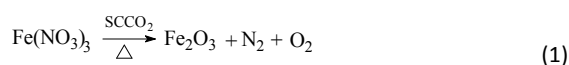

Figure 2. (a) TEM image and wide-survey XPS spectrum of GO sheet. (b) TEM image and wide-survey XPS spectrum of Fe_2O_3/Graphene nanocomposite. (c) High resolution TEM image of Fe_2O_3/Graphene nanocomposite sheet. (d) XRD pattern of the Fe_2O_3/Graphene nanocomposite. (e) Hysteresis loop of Fe_2O_3/Graphene nanocomposite. The inset is optical images of magnetism measurement for Fe_2O_3/Graphene nanocomposite. The left corner image is the Fe_2O_3/Graphene nanocomposite aqueous solution. The Tyndall effect reveals the homogeneous dispersion of Fe_2O_3/Graphene nanocomposite in aqueous solution. The right corner image is the Fe_2O_3/Graphene nanocomposite aqueous solution after magnet removed.

We started characterization after the first step of the fabrication to observe the structure of Fe_2O_3/Graphene nanosheets by using transmission electron microscopy (H-600 TEM, Hitachi, Japan). As compared to the structure of GO (shown in Figure 2a), it can be clearly observed that graphene is uniformly coated by Fe_2O_3 nanoparticles (Figure 2b). Furthermore, Figure 2c shows a high magnification TEM image of Fe_2O_3/Graphene nanocomposites,

which clearly exhibits that the graphene surface is uniformly covered by Fe_2O_3 nanoparticles of several nanometers in diameter. An X-ray diffraction (XRD) analysis was used to determine the crystal structure of the Fe_2O_3/Graphene nanosheet sample. As shown in Figure 2d, the resolved diffraction peaks are closely indexed to pure hexagonal α-Fe2O3. This perfectly matches the standard α-Fe2O3 sample (Joint Committee on Powder Diffraction Standards (JCPDS) card No. 33-0664), which indicates that the as prepared sample is α-Fe_2O_3. Similar to the standard XRD pattern of bulk α-Fe_2O_3, the peak intensities of diffraction planes (104) and (110) in the XRD pattern of the sample are relatively higher than other diffraction peaks.[17] For comparison, we performed the same experiment in the absence of GO, where aggregation of large particles of Fe_2O_3 was observed (see Supporting Information, Figure S1). Thus, in the absence of GO, only aggregated Fe_2O_3 nanoparticles were obtained, which suggests that GO is capable of stabilizing Fe_2O_3 nanoparticles by preventing their aggregation. Furthermore, the effect of $Fe(NO_3)_3 \cdot 9H_2O$ on the nanocomposite morphologies were also investigated (see Supporting Information, Figure S2).

The formation of Fe_2O_3 in the nanocomposite is verified by X-ray photoelectron spectroscopy (XPS) measurements which are carried out on a FEI Sirion 200 spectrometer, using monochromatic Al *Kα* radiation at 12.5 keV and 300 W. Pass energy of 300 eV was used for the survey spectra. Take-off-angles relative to sample surface of 45° was employed. Wide-survey XPS spectrum (Figure 2a) of the GO demonstrated the predominant presence of carbon (68.32 at.%) and oxygen (31.68 at.%). As shown in Figure 2b, the wide-survey XPS spectrum of as-prepared composites contains the predominant presence of carbon (67.90 at.%), oxygen (20.30 at.% for graphene, 7.08 at.% for Fe_2O_3), and iron (4.72 at.%). No nitrogen or other elements were detectable, which suggests that there were no byproducts or unreacted precursors in the nanocomposite. Furthermore, the contents of both carbon and oxygen were found decreased in the composite, compared to that of GO. The decrease of carbon may be due to the decarboxylation reaction, and the significantly decrease of oxygen is related to the dehydration reaction, which is main reaction occurred in the formation of

Fe_2O_3/Graphene nanocomposite from GO, while GO is reduced. On the basis of previously reported studies[17,18,19], a possible mechanism is proposed here as following:

$$Fe(NO_3)_3 \xrightarrow[\triangle]{SCCO_2} Fe_2O_3 + N_2 + O_2 \tag{1}$$

$$GO(-OH, -COOH) \xrightarrow[\triangle]{SCCO_2} Graphene \tag{2}$$

$$Fe_2O_3 + Graphene \xrightarrow[\triangle]{SCCO_2} Fe_2O_3/graphene\ nanocomposite \tag{3}$$

Since the GO surface is negatively charged in solution because of oxygen functional groups, the Fe ions are firstly adsorb on GO surface due to the electrostatic force. Then the above chemical reactions occurred.[20, 21] Equation 1 represents the formation of Fe_2O_3 with the aid of heat. As reported, Fe_2O_3, N_2O_5 and O_2 are all formed in 120 ℃, while the formation of N_2 requires higher temperature around 350 ℃ or higher. Equation 2 represents the transformation of graphene from GO with the aid of heat. The heat treatment can promote the dehydration reaction. Equation 3 shows the formation of Fe_2O_3/Graphene nanocomposite. From the minimum energy point of view, the initially generated Fe_2O_3 may attach to the surface of GO. Then, these Fe_2O_3 can act as nuclei for the further particle growth in the heat treatment. Note that there is no clear reaction order for the reaction of 1, 2 and 3. These reactions may be happening simultaneously after 60 ℃, which was investigated in our previous study[22]. Meanwhile, magnetism measurement for the Fe_2O_3/Graphene nanocomposite was also performed, as shown in Figure 2e. As seen from the inset image in Figure 2e, Fe_2O_3/Graphene nanosheets are obediently moved toward the magnet. The coercive force of the Fe_2O_3/Graphene nanocomposite is found to be about 1275.5 Oe, and the remanence is about 17.6 mT.
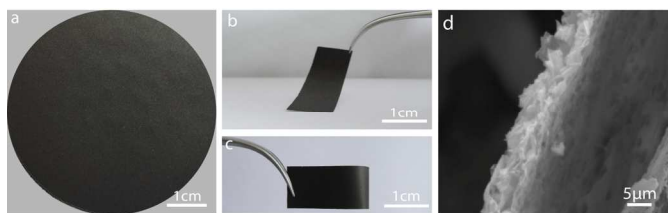
Figure 3. Morphology and structure of Fe$_2$O$_3$/Graphene paper. (a–c) Digital camera images of Fe$_2$O$_3$/Graphene paper. (a) flat ~6μm thick, (b and c) folded ~6μm thick film (the red square indicate the zoom place for d). (d) SEM side-view images of ~6μm thick sample (see Supporting Information, Figure S3).

After completing Fe$_2$O$_3$/Graphene nanosheets' characterization, second step of the fabrication and thence second step of characterization was initiated. After the second step of the fabrication resulting carbon based paper was almost black (Figure 3a) and exhibited excellent flexibility (Figure 3b and c). The fracture edges of a VAFe/GN paper investigated via scanning electron microscopy (SEM). SEM observations revealed well vertical arrangement of Fe$_2$O$_3$/Graphene nanosheets through almost the entire cross-section of the paper (Figure 3d).

To determine whether the obtained VAFe/GN could be used as a sensor for H$_2$S, their CL characteristics in response to H$_2$S were investigated by procedures similar to those reported in our previous work.[23] VAFe/GN paper was put into a quartz tube with the inner diameter of 12 mm. The air from the pump mixed with H$_2$S and flowed through the quartz tube automatically, H$_2$S was oxidized on the surface of catalyst by the oxygen in air. The consequent CL intensity was directly measured with a BPCL ultra weak chemiluminescence analyzer.

For comparison, graphene paper is also fabricated using traditional filtration method.[24] Figure 4a (black curve) shows the sensing characteristic of graphene paper in response to H$_2$S at 190℃. Almost no CL signal has been detected except some noise from the radiation of the substrate during the measurement. The HAFe/GN paper, however, demonstrates well response to H$_2$S gas, as seen in Figure 4b (dark grey curve). The HAFe/GN device exhibits CL emission of

about 350 absorption units in response to 23 ppm H$_2$S at 190 ℃. This CL intensity is almost comparable to that of CNT based sensor in response to 100 ppm H$_2$S at 360 ℃.[17, 23] More interestingly, the VAFe/GN paper device exhibits more sensitivity than that of HAFe/GN device. Figure 4b (grey curve) shows the sensor characteristics of the as-prepared VAFe/GN paper in response to H$_2$S. The sensor exhibits significant CL emission of about 450 absorption units in response to 15 ppm H$_2$S at 190 ℃. Furthermore, the obtained sensor also has short response time about 500 μs and fast recovery time of less than 30 s, as well as good reproducibility with relatively minor deviations for four replicate injections of 15 ppm H$_2$S at 190 ℃. Additionally, it is noteworthy that the detection limit of the as-prepared VAFe/GN is lower than 10 ppm H$_2$S at 130 ℃ (see Supporting Information, Figure S4). The performances of fast response, lower detection limit and rapid recovery may further widen the applications of VAFe/GN in industrial field. The excellent response performances of VAFe/GN may stem from not only the large amount of the uniformly distributed Fe$_2$O$_3$ on graphene sheets, but also the special structure of vertical arrangement of Fe$_2$O$_3$/Graphene nanosheets (as seen in Figure 4c and d). Obviously, the special structure of VAFe/GN paper can provide larger contact area for the detective gas, and less resistive to the flow i.e. the VAFe/GN paper is more sensitive to H$_2$S gas. The efficiency of Fe$_2$O$_3$/Graphene nanocomposite device for H$_2$S response are schematically shown in Figure 4e and f.
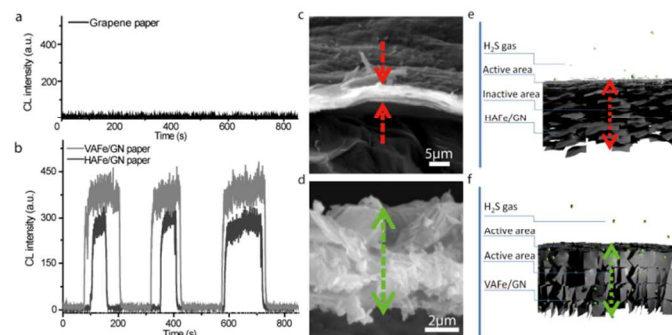

Figure 4. Response curves of H$_2$S on (a) graphene paper, (b) HAFe/GN paper, and the as-prepared VAFe/GN paper. The air flow rate is 200 ml/min. The H$_2$S is automatically injected. (c) SEM image for HAFe/GN paper (additional cross sectional SEM image of the HAFe/GN, see Supporting Information, Figure S5). (d) SEM

image for VAFe/GN paper. (the top view image, see in Supporting Information, Figure S6). (e and f) Scheme for the gas response efficiency of Fe_2O_3/Graphene nanocomposite device. (e) HAFe/GN paper. (f) VAFe/GN paper.

In addition, the VAFe/GN paper sensor was evaluated with a variety of other gases, including carbon dioxide, ethanol, benzene and toluene, with temperatures ranging from 100℃ to 300℃. None of these gases gave any detectable CL signals, which suggests the high selectivity of the sensor for H_2S.

Conclusions

In summary, we have fabricated Fe_2O_3/Graphene nanosheets and shown that they can be aligned either vertically or horizontally depending on the external magnetic field. Later produced VAFe/GN and HAFe/GN papers have not only well flexibility but also excellent response performances to H_2S gas with high selectivity which demonstrates their potential use as facile, low-cost and high efficiency H_2S sensors. Comparison between VAFe/GN and HAFe/GN papers' response to H_2S gas yields that structural orientation of nanosheets plays an essential role in maximizing the efficiency. Besides what we have investigated in this study, one of the most preferred uses of Fe_2O_3/Graphene nanocomposites is to enhance Li-Ion storage properties;[25-27] we believe that researcher working on this topic could benefit from our findings.[28-30] Furthermore, the method we used can be easily expanded to the fabrication of other functional graphene nanosheet arrays, such as serving as template for producing hybrid materials containing polymers, ceramics and metals.

Notes and references

[a] Department of Polymer Science and Technology, School of Chemical Engineering and Technology, Harbin Institute of Technology, 150001 Harbin, People's Republic of China

[b] Interdisciplinary Nanoscience Center (iNANO), Aarhus University, DK-8000, Aarhus C, Denmark

[c] Regional Centre of Advanced Technologies and Materials, Department of Physical Chemistry, Faculty of Science, Palacký University, 77146 Olomouc, Czech Republic

[†] These authors contributed equally to this work.

[*] To whom correspondence should be addressed.
  E-mail: huangyd@hit.edu.cn and dong@inano.au.dk

Acknowledgments

1. Z. J. Fan, J. Yan, L. J. Zhi, Q. Zhang, T. Wei, J. Feng, M. L. Zhang, W. Z. Qian and F. Wei, *Adv Mater*, 2010, **22**, 3723-3726.
2. L. Jabbour, C. Gerbaldi, D. Chaussy, E. Zeno, S. Bodoardo and D. Beneventi, *J Mater Chem*, 2010, **20**, 7344-7347.
3. D. W. Wang, F. Li, J. P. Zhao, W. C. Ren, Z. G. Chen, J. Tan, Z. S. Wu, I. Gentle, G. Q. Lu and H. M. Cheng, *Acs Nano*, 2009, **3**, 1745-1752.
4. Z. F. Ren, Z. P. Huang, J. W. Xu, J. H. Wang, P. Bush, M. P. Siegal and P. N. Provencio, *Science*, 1998, **282**, 1105-1107.
5. S. H. Hong, J. Zhu and C. A. Mirkin, *Science*, 1999, **286**, 523-525.
6. M. Aryal, K. Trivedi and W. C. Hu, *Acs Nano*, 2009, **3**, 3085-3090.
7. T. Zhang, Q. Xue, S. Zhang and M. Dong, *Nano Today*, 2012, **7**, 180-200.
8. P. Lazar, S. Zhang, K. Šafářová, Q. Li, J. P. Froning, J. Granatier, P. Hobza, R. Zbořil, F. Besenbacher, M. Dong and M. Otyepka, *ACS Nano*, 2013, **7**, 1646-1651.
9. X. Zhong, H. Yu, G. Zhuang, Q. Li, X. Wang, Y. Zhu, L. Liu, X. Li, M. Dong and J.-g. Wang, *J Mater Chem A*, 2014, **2**, 897-901.
10. Z. Jiang, D. Xia, Y. Li, J. Li, Q. Li, M. Chen, Y. Huang, F. Besenbacher and M. Dong, *Nanotechnology*, 2013, **24**, 335704.
11. Z. Jiang, Q. Li, M. Chen, J. Li, J. Li, Y. Huang, F. Besenbacher and M. Dong, *Nanoscale*, 2013, **5**, 6265-6269.
12. Y. Li, Y. Yu, J.-G. Wang, J. Song, Q. Li, M. Dong and C.-J. Liu, *Appl Catal B Environ*, 2012, **125**, 189-196.
13. S. Jiang, A. A. Eltoukhy, K. T. Love, R. Langer and D. G. Anderson, *Nano Lett*, 2013, **13**, 1059-1064.

14. L. Gao, L. Xie, X. Long, Z. Wang, C.-Y. He, Z.-Y. Chen, L. Zhang, X. Nan, H. Lei, X. Liu, G. Liu, J. Lu and B. Qiu, *Biomaterials*, 2013, **34**, 3688-3696.

15. W. A. Ang, N. Gupta, R. Prasanth, H. H. Hng and S. Madhavi, *J Mater Res*, 2013, **28**, 824-831.

16. J. Chen, L. N. Xu, W. Y. Li and X. L. Gou, *Adv Mater*, 2005, **17**, 582-586.

17. Z. Y. Sun, H. Q. Yuan, Z. M. Liu, B. X. Han and X. R. Zhang, *Adv Mater*, 2005, **17**, 2993-2996.

18. G. M. An, W. H. Ma, Z. Y. Sun, Z. M. Liu, B. X. Han, S. D. Miao, Z. J. Miao and K. L. Ding, *Carbon*, 2007, **45**, 1795-1801.

19. Z. X. Jiang, J. J. Wang, L. H. Meng, Y. D. Huang and L. Liu, *Chem Commun*, 2011, **47**, 6350-6352.

20. S. M. Cui, Z. H. Wen, E. C. Mattson, S. Mao, J. B. Chang, M. Weinert, C. J. Hirschmugl, M. Gajdardziska-Josifovska and J. H. Chen, *J Mater Chem A*, 2013, **1**, 4462-4467.

21. S. Mao, S. M. Cui, G. H. Lu, K. H. Yu, Z. H. Wen and J. H. Chen, *J Mater Chem*, 2012, **22**, 11009-11013.

22. Z. Y. Sun, Z. M. Liu, Y. Wang, B. X. Han, J. M. Du and J. L. Zhang, *J Mater Chem*, 2005, **15**, 4497-4501.

23. Z. Y. Zhang, H. J. Jiang, Z. Xing and X. R. Zhang, *Sensor Actuat B-Chem*, 2004, **102**, 155-161.

24. D. Li, M. B. Muller, S. Gilje, R. B. Kaner and G. G. Wallace, *Nat Nanotechnol*, 2008, **3**, 101-105.

25. D. H. Wang, D. W. Choi, J. Li, Z. G. Yang, Z. M. Nie, R. Kou, D. H. Hu, C. M. Wang, L. V. Saraf, J. G. Zhang, I. A. Aksay and J. Liu, *Acs Nano*, 2009, **3**, 907-914.

26. G. M. Zhou, D. W. Wang, F. Li, L. L. Zhang, N. Li, Z. S. Wu, L. Wen, G. Q. Lu and H. M. Cheng, *Chem Mater*, 2010, **22**, 5306-5313.

27. D. H. Wang, R. Kou, D. Choi, Z. G. Yang, Z. M. Nie, J. Li, L. V. Saraf, D. H. Hu, J. G. Zhang, G. L. Graff, J. Liu, M. A. Pope and I. A. Aksay, *Acs Nano*, 2010, **4**, 1587-1595.

28. J. K. Lee, K. B. Smith, C. M. Hayner and H. H. Kung, *Chem Commun*, 2010, **46**, 2025-2027.

29. D. Y. Pan, S. Wang, B. Zhao, M. H. Wu, H. J. Zhang, Y. Wang and Z. Jiao, *Chem Mater*, 2009, **21**, 3136-3142.

30. B. J. Li, H. Q. Cao, J. Shao, M. Z. Qu and J. H. Warner, *J Mater Chem*, 2011, **21**, 5069-5075.

Journal of Materials Chemistry A Accepted Manuscript